ENGINEERING TRANSACTIONS • *Engng. Trans.* • **45**, 1, 91–101, 1997
Polish Academy of Sciences • Institute of Fundamental Technological Research
10.24423/engtrans.683.1997

A NOTE ON THE NUMERICAL MODELLING OF VISCOPLASTIC DAMAGE

P. KŁOSOWSKI (GDAŃSK)

R. SCHMIDT and D. WEICHERT (AACHEN)

In this paper, a numerical model of the viscoplastic behaviour of metals including damage effects is proposed. The Chaboche model of constitutive equations accounting for viscoplasticity coupled to damage is applied. Three types of uniaxial tests are presented: constant strain rate tests, creep tests, and cyclic loading tests. Numerical results for rupture under cyclic loading are compared to experimental results given in [1]. Results of calculations based on pure viscoplastic material behaviour are compared to those including damage effects. The present investigations are preliminary to the implementation of the proposed model into more general FEM codes.

1. Introduction

The numerical modelling of material damage by means of continuum mechanics applied to a one-dimensional structural element is the subject of this paper. Out of a great number of areas of potential application of the present general model, the problems of life prediction, assessment of safety and reliability of aeronautical structures, piping, pressure vessels, power plants or jet engines can be mentioned. Usually, before carrying out experiments on real structures, uniaxial experiments are performed. In the same sense, a more general numerical model developed by the authors is checked by application to truss elements.

In [2], the description of different models of material damage can be found. Here we restrict ourselves to the viscoplastic type of damage, which is an appropriate choice for metals at high temperatures in combination with viscoplastic constitutive equations. In the literature of damage analysis, most often the CHABOCHE [1, 3–6], the Bodner-Partom [7, 8], and the GURSON theories of damage [9] are applied. More sophisticated damage approaches, taking into account anisotropy of the material during the deformation process, are presented in [10, 11]. Instead of scalar damage variables, anisotropic damage models use vectors and tensors of second or higher order as internal state variables. Only a few papers with results of uniaxial experiments on viscoplastic specimens were available to the authors [1, 7, 12, 13]. Some of them include a comparison of

experimental and numerical results, taking also damage effects into account [1, 7, 12]. The aim of the present paper is to compare the results of numerical simulations to available experimental results and to check the influence of damage on the viscoplastic behaviour of INCO alloy specimens. Also, the influence of the temperature is studied for isothermal states.

2. Characterisation of the damage model

Here, we will deal numerically with the uniaxial problem only. Therefore, in this chapter we present the uniaxial form of the governing equations, parallel to the general description. We assume that strains are small enough so that the additive decomposition of total strain rates into the elastic and inelastic part is justified. So, the total Green - Lagrange strain rate tensor $\dot{\boldsymbol{\varepsilon}}$ can be written in the form

$$\dot{\boldsymbol{\varepsilon}} = \dot{\boldsymbol{\varepsilon}}^e + \dot{\boldsymbol{\varepsilon}}^i, \qquad \dot{\varepsilon} = \dot{\varepsilon}^e + \dot{\varepsilon}^i, \tag{2.1}$$

where $\dot{\boldsymbol{\varepsilon}}^e$ and $\dot{\boldsymbol{\varepsilon}}^i$ are the elastic and inelastic strain rates, respectively. For isotropic materials the relation between the rate of the second Piola - Kirchhoff stress tensor and the elastic part of the strain rate tensor can be expressed by

$$\dot{\boldsymbol{\sigma}} = \mathbf{E} : \dot{\boldsymbol{\varepsilon}}^e, \qquad \dot{\sigma} = E\dot{\varepsilon}^e. \tag{2.2}$$

Here, $\mathbf{E}$ denotes the tensor of elastic moduli, E is Young's modulus. Using (2.1), equation (2.2) can be transformed into:

$$\dot{\boldsymbol{\sigma}} = \mathbf{E} : \left(\dot{\boldsymbol{\varepsilon}} - \dot{\boldsymbol{\varepsilon}}^i\right), \qquad \dot{\sigma} = E\left(\dot{\varepsilon} - \dot{\varepsilon}^i\right). \tag{2.3}$$

We assume isotropic damage, which means that cracks and cavities appearing during deformation are distributed uniformly in all directions. In this case the effect of damage can be expressed by the scalar parameter $D \in [0, 1]$, which defines the relation between the apparent stress and the effective stress tensors $\overline{\boldsymbol{\sigma}}$

$$\overline{\boldsymbol{\sigma}} = \boldsymbol{\sigma}/(1 - D), \qquad \overline{\sigma} = \sigma/(1 - D). \tag{2.4}$$

The inelastic strain rates are given by:

$$\dot{\boldsymbol{\varepsilon}}^i = \frac{3}{2}\dot{p}\frac{\boldsymbol{\sigma}' - \mathbf{X}}{J(\boldsymbol{\sigma}' - \mathbf{X}')}, \qquad \dot{\varepsilon}^i = \dot{p} \cdot \operatorname{sign}(\sigma - X), \tag{2.5}$$

where $\dot{p}$ is the rate of the equivalent plastic strain, $\mathbf{X}$ is the backstress tensor, $(\cdot)'$ denotes the deviatoric part of the respective tensor, and J stands for the

second invariant of the argument:

$$J(\boldsymbol{\sigma}' - \mathbf{X}') = \left(\frac{3}{2}(\boldsymbol{\sigma}' - \mathbf{X}') : (\boldsymbol{\sigma}' - \mathbf{X}')\right)^{1/2},$$

$$J(\boldsymbol{\sigma}' - \mathbf{X}') = J\left(\begin{bmatrix} \frac{2}{3}(\sigma - X) & 0 & 0 \\ 0 & -\frac{1}{3}(\sigma - X) & 0 \\ 0 & 0 & -\frac{1}{3}(\sigma - X) \end{bmatrix}\right) = |\sigma - X|. \tag{2.6}$$

In the Chaboche model of viscoplasticity coupled to damage, the rate of the equivalent plastic strain $\dot{p}$ is defined by [1, 2]:

$$\begin{aligned} \dot{p} &= \gamma \left\langle \frac{J(\boldsymbol{\sigma}' - \mathbf{X}')/(1-D) - R - k}{K} \right\rangle^n, \\ \dot{\varepsilon}^i &= \gamma \left\langle \frac{|\sigma - X)/(1-D) - R - k}{K} \right\rangle^n \operatorname{sign}(\sigma - X). \end{aligned} \tag{2.7}$$

Here k, K, and n, are material parameters to be determined by experiments, D is the damage parameter, and $\langle x \rangle$ is the McCauley bracket defined by $\langle x \rangle = 1/2(x + |x|)$. In the typical Chaboche's approach the parameter $\gamma = 1.0$. The material parameter K is related to the parameter μ given in [1]

$$K = \mu^{-1/n}. \tag{2.8}$$

The scalar R and the backstress tensor $\mathbf{X}$ represent isotropic and kinematic hardening. Their evolution is defined by

$$\dot{R} = b(R_1 - R)\dot{p}, \qquad \dot{R} = b(R_1 - R)\left|\dot{\varepsilon}^i\right|, \tag{2.9}$$

$$\dot{\mathbf{X}} = \frac{2}{3}a\dot{\boldsymbol{\varepsilon}}^i - c\mathbf{X}\dot{p}, \qquad \dot{X} = \frac{2}{3}a\dot{\varepsilon}^i - cX\left|\dot{\varepsilon}^i\right|, \tag{2.10}$$

where b, R_1, a, and c are hardening parameters. If in Eq. (2.7) we assume no hardening and additionally $\gamma \neq 1.0$, the Perzyna type of elasto-viscoplastic constitutive equations can be easily obtained.

According to [1], the damage evolution is assumed in the form:

$$\dot{D} = \left[-\frac{Y}{S}\right]^s \dot{p}, \qquad \dot{D} = \left[-\frac{Y}{S}\right]^s \left|\dot{\varepsilon}^i\right|, \tag{2.11}$$

$$\begin{aligned} -Y &= \frac{1}{2(1-D)^2 E}\left[\frac{2}{3}(1+\nu)\sigma_{\text{equ}}^2 + 3(1-2\nu)\sigma_H^2\right], \\ -Y &= \frac{1}{2(1-D)^2 E}\left[\frac{2}{3}(1+\nu)\sigma_{\text{equ}}^2\right] \end{aligned} \tag{2.12}$$

with

$$\sigma_{\text{equ}} = \left[\frac{3}{2}\boldsymbol{\sigma}' : \boldsymbol{\sigma}'\right]^{1/2},$$

$$\sigma_{\text{equ}} = \left[\frac{3}{2}\left(\frac{2}{3}\sigma\cdot\frac{2}{3}\sigma + \left(-\frac{1}{3}\sigma\right)\cdot\left(-\frac{1}{3}\sigma\right) + \left(-\frac{1}{3}\sigma\right)\cdot\left(-\frac{1}{3}\sigma\right)\right)\right]^{1/2} = \sigma, \tag{2.13}$$

$$\sigma_H = \frac{1}{3}\text{Tr}(\boldsymbol{\sigma}), \qquad \sigma_H = \frac{1}{3}\left(\frac{2}{3}\sigma - \frac{1}{3}\sigma - \frac{1}{3}\sigma\right) = 0, \tag{2.14}$$

where s and S are material parameters to be determined by experiments.

Equations (2.7), (2.9)–(2.11) have differential form. Including them into a computer algorithm requires the choice of an appropriate numerical method of time integration. In the present work the trapezoidal method was used because of its simplicity. It is based on the following equations

$$\Delta\boldsymbol{\chi} = \frac{\Delta t}{2}\left[f(\boldsymbol{\sigma}_{t-\Delta t}, \mathbf{X}_{t-\Delta t}, R_{t-\Delta t}, D_{t-\Delta t}) + f(\boldsymbol{\sigma}_t, \mathbf{X}_t, R_t, D_t)\right]$$

$$= \frac{\Delta t}{2}\left[\dot{\boldsymbol{\chi}}_{t-\Delta t} + \dot{\boldsymbol{\chi}}_t^{k-1}\right], \tag{2.15}$$

$$\boldsymbol{\chi} \in \left(\boldsymbol{\varepsilon}^i, \mathbf{X}, R, D\right).$$

For a certain time increment Δt in the iteration process (with k denoting the number of the iteration) one obtains the current values of the integrated functions by the relations:

$$\boldsymbol{\varepsilon}_t^i = \boldsymbol{\varepsilon}_t^{ik} = \boldsymbol{\varepsilon}_{t-\Delta t}^i + \Delta\boldsymbol{\varepsilon}^i, \qquad \mathbf{X}_t = \mathbf{X}_t^k = \mathbf{X}_{t-\Delta t} + \Delta\mathbf{X},$$
$$R_t = R_t^k = R_{t-\Delta t} + \Delta R, \qquad D_t = D_t^k = D_{t-\Delta t} + \Delta D. \tag{2.16}$$

The chosen time increment must be small enough to guarantee the convergence of the iteration process. According to [14] it must fulfil the condition

$$\frac{1}{2}\Delta t\left\|\frac{\partial\boldsymbol{\chi}}{\partial\mathbf{y}_n}\right\| < 1, \qquad \mathbf{y}_n \in (\boldsymbol{\sigma}, \mathbf{X}, R, D). \tag{2.17}$$

The iterations process is carried out until for the inelastic strain rate $\dot{\varepsilon}^i$ the error is lower than the assumed error range η

$$\left|\frac{\dot{\varepsilon}_t^{ik} - \dot{\varepsilon}_t^{ik-1}}{\dot{\varepsilon}_t^{ik}}\right| < \eta. \tag{2.18}$$

Details of the algorithm of the numerical procedure can be found in [15, 16].

3. Numerical results

The numerical simulations were performed for uniaxial loading of truss element-shaped INCO alloy specimens (length $l = 1.0\,\mathrm{m}$, cross-section area $A = 0.0001\,\mathrm{m}^2$). Material parameters for different temperatures calculated from formulas given in [1] are given in Table 1.

Table 1.

Temperature		165° C	300° C	450° C	627° C
E	GPa	$197{\cdot}10^3$	$189{\cdot}10^3$	$178{\cdot}10^3$	$162{\cdot}10^3$
ν	–	0.3	0.3	0.3	0.3
K	$\mathrm{MPa}^{1/n}$	699	1634	4200	12790
k	MPa	874	813	708	501
n	–	2.4	2.4	2.4	2.4
a	GPa	80	80	80	80
c	–	200	200	200	200
R_1	MPa	−8.97	−24.81	−61.92	−165.4
b	–	15	15	15	15
s	–	3.0	3.0	3.0	3.0
S	MPa	8.55	7.36	6.04	4.48

Three types of numerical tests were performed: constant strain rate tests, creep tests and the cyclic loading tests. For each of them the results based on pure viscoplastic material behaviour are compared to those including viscoplastic damage effects. In the plots for the constant strain rate and creep tests the critical damage ($D = 0.24$) is indicated, which is considered as a limit of the present theory.

In Fig. 1 A plots of the stress versus strain obtained for different strain rates at $T = 627°$ C are shown. For small strain rates only a small influence of damage can be observed. Also for higher strain rates the plots obtained on the basis of constitutive equations with and without damage are nearly identical, but the critical value of damage is reached. The evolution of the damage parameter is shown in Fig. 1 B. The critical damage is first obtained for the strain rate $\dot{\varepsilon} = 0.01\,\mathrm{s}^{-1}$; for both higher and lower strain rates the critical value of damage is reached at larger strains.

Results for the numerical simulation of creep tests for the same type of specimens are presented in Fig. 2. In Fig. 2 A plots of the strain versus time are given for different levels of stress. For stresses up to $\sigma = 1500\,\mathrm{MPa}$ there is no difference between elasto-viscoplastic and elasto-viscoplastic damage analysis. The damage effect becomes more important for high stress levels (when the applied

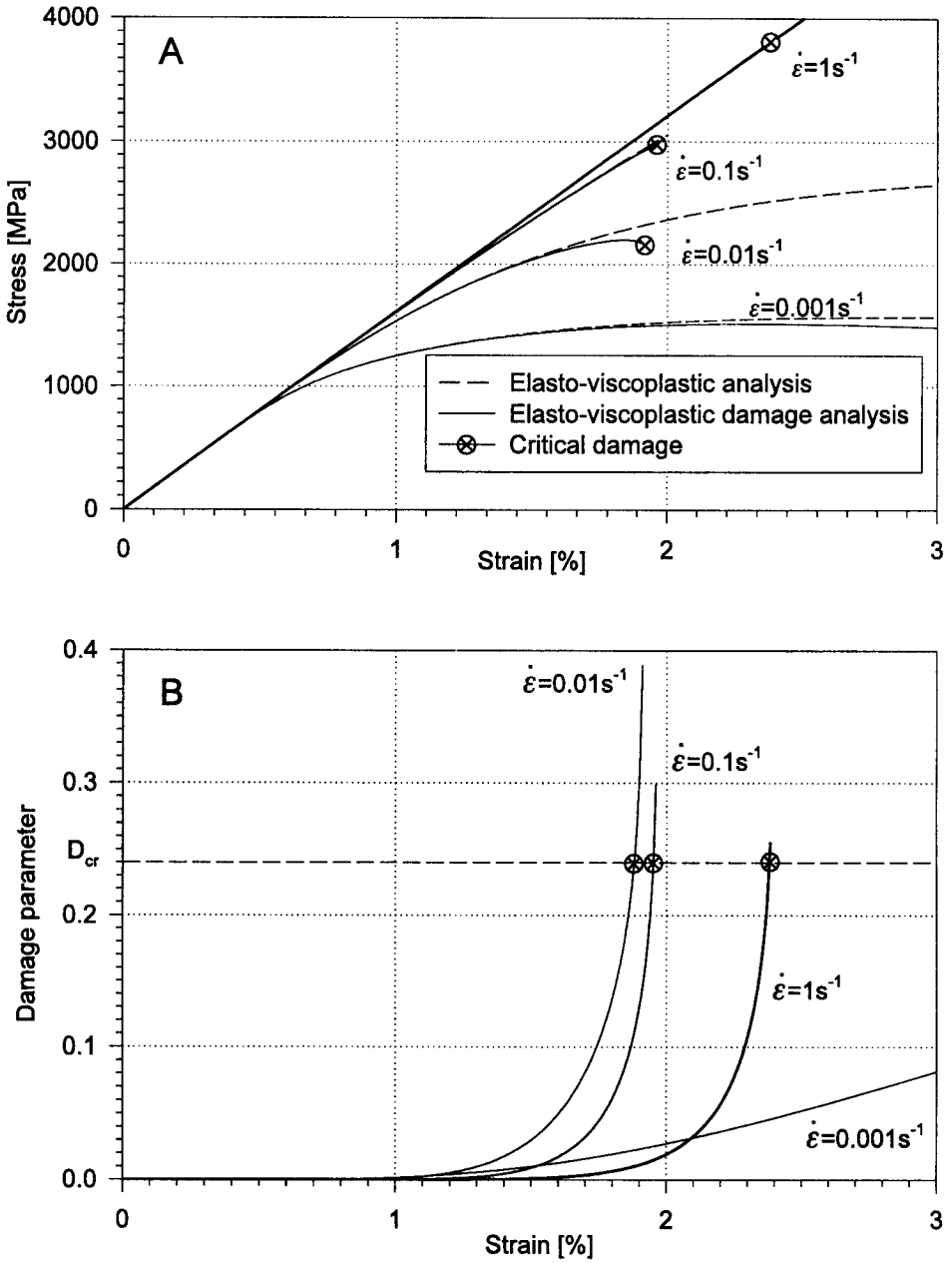

FIG. 1. Constant strain rate tests for INCO specimens at $T = 627°$ C. A) Stress, B) damage parameter.

load causes stresses beyond the hardening saturation value). Only in this case (see Fig. 2 B) the critical damage value is reached.

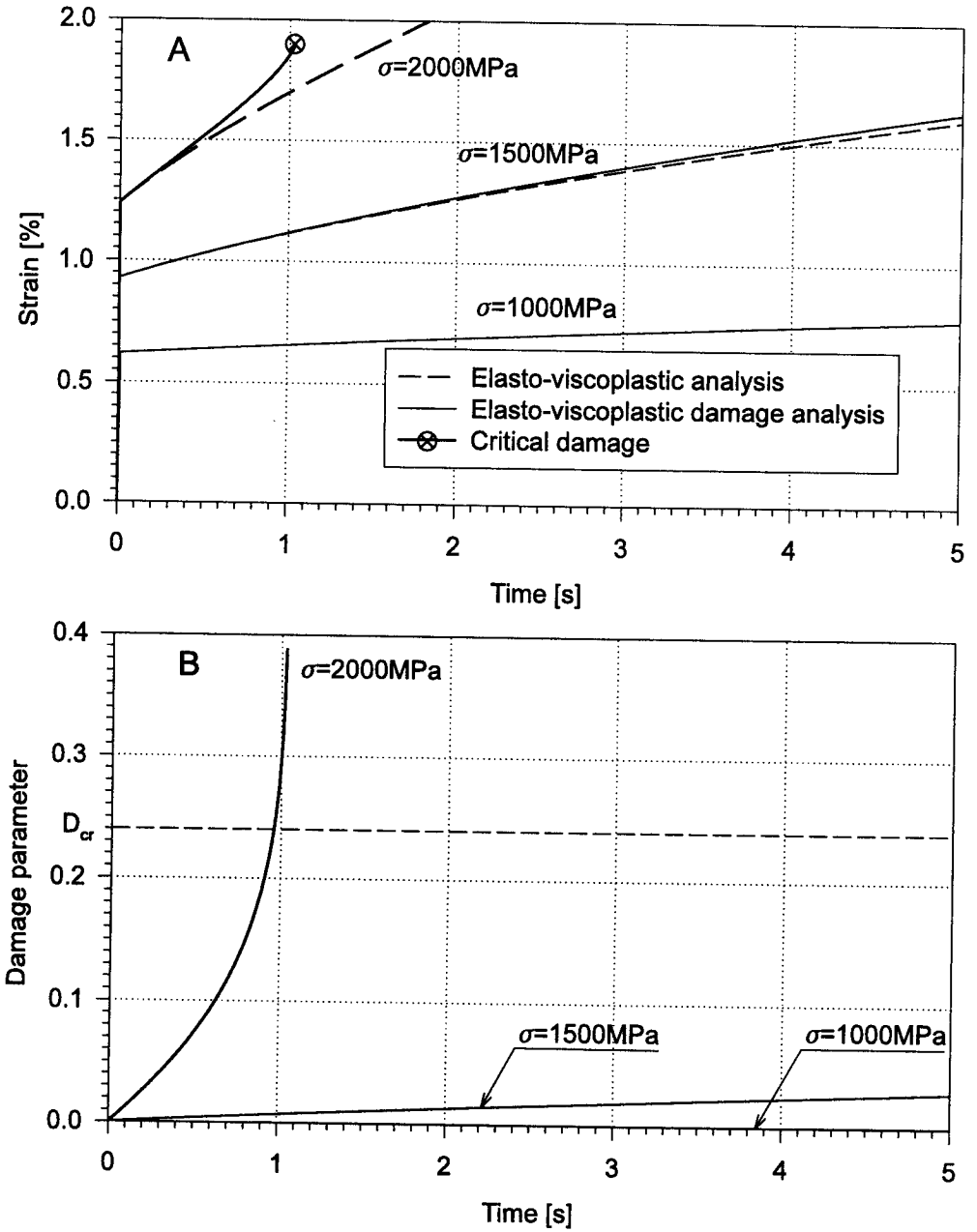

FIG. 2. Creep tests for INCO specimens at $T = 627°$ C. A) Strain, B) damage parameter.

In Fig. 3 the numerical results for cyclic tests are compared to experimental results available in [1]. The tests were carried out for different strain ranges $\Delta\varepsilon$ and different temperatures. Each test was performed with the constant strain

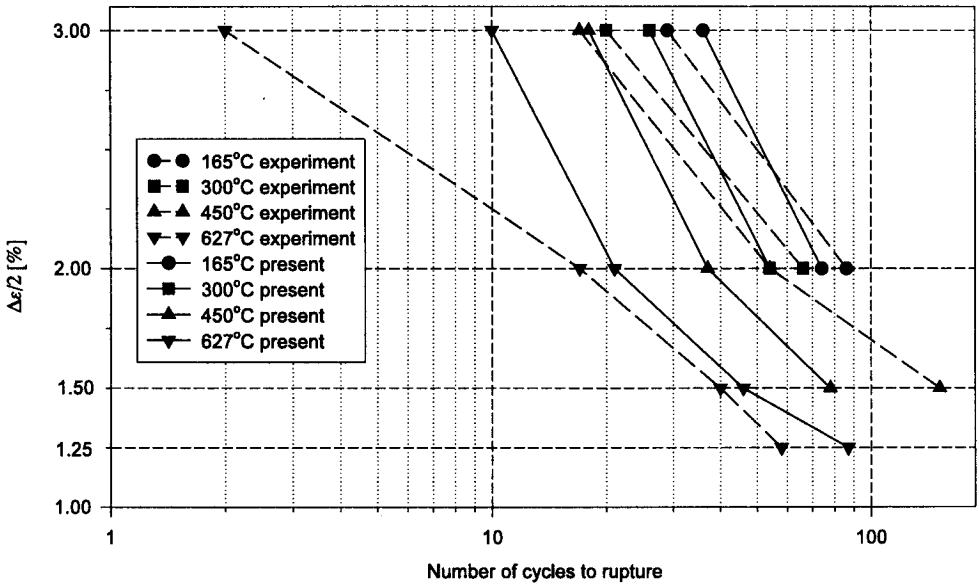

FIG. 3. Cyclic tests for INCO specimens. Number of cycles to rupture.

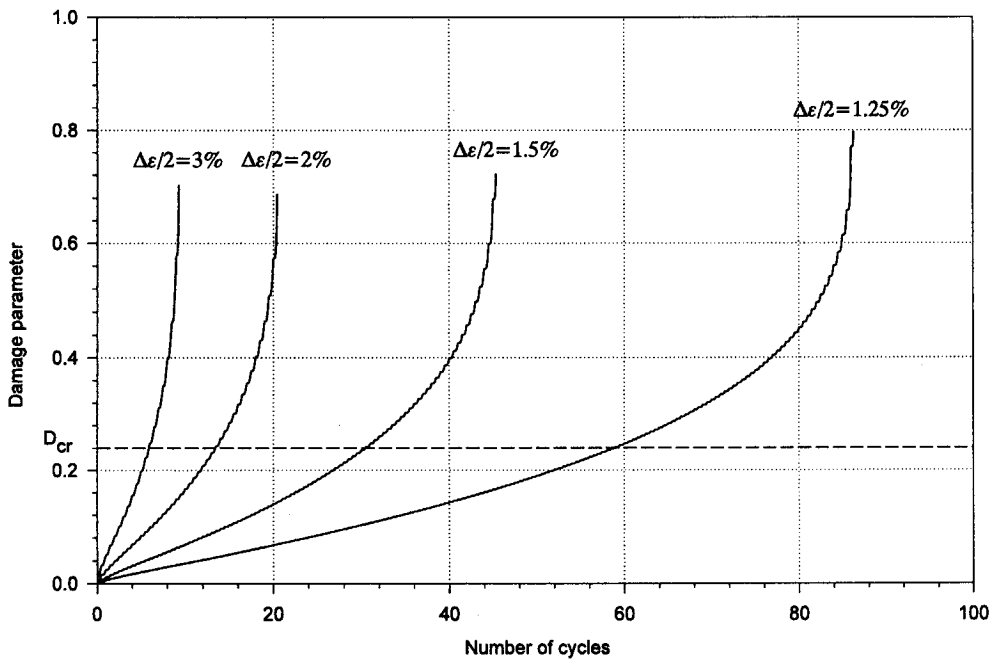

FIG. 4. Cyclic tests for INCO specimens at $T = 627°$ C with $\dot{\epsilon} = 10^{-5}$ 1/s. Evolution of the damage parameter.

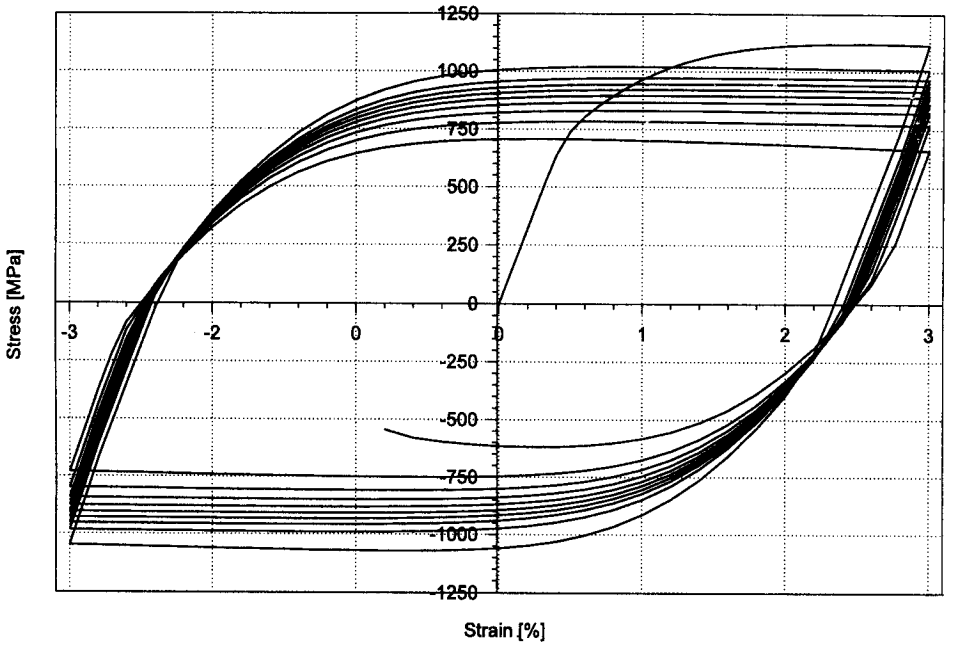

FIG. 5. Cyclic test for an INCO specimen at $T = 627°$ C with $\Delta\varepsilon/2 = 3\%$ and $\dot{\varepsilon} = 10^{-5}$ 1/s.

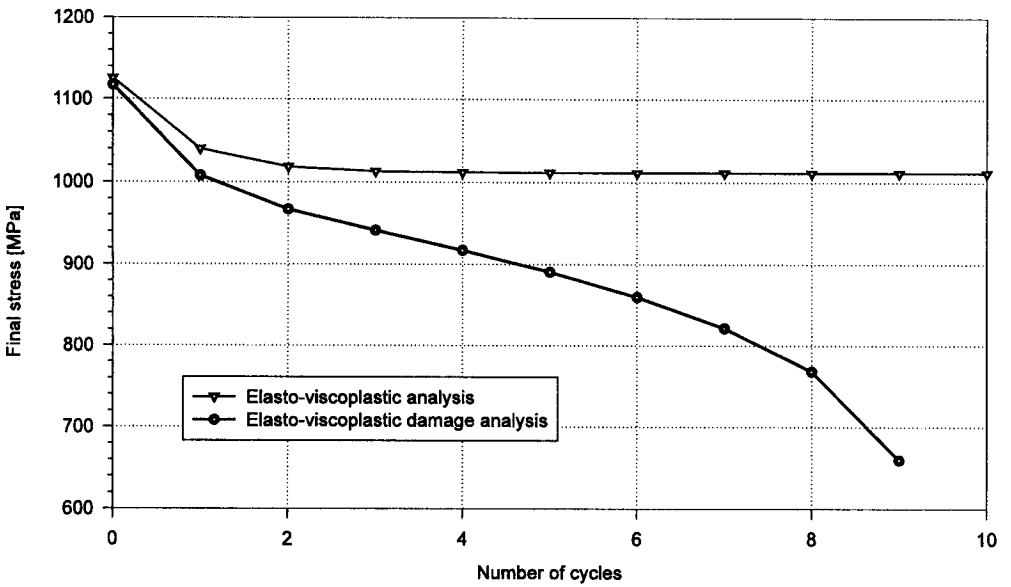

FIG. 6. Cyclic test for an INCO specimen at $T = 627°$ C with $\Delta\varepsilon/2 = 3\%$ and $\dot{\varepsilon} = 10^{-5}$ 1/s. Change of final stress at $\Delta\varepsilon/2 = 3\%$.

rate $\dot{\varepsilon} = 10^{-5}\,1/\mathrm{s}$. In Fig. 3 the number of cycles necessary for rupture of the specimen is given. Rupture is here assumed to occur if the calculated value of the damage parameter D is equal to 1.0. A fair correlation of the numerical results with the experiments can be observed. The authors are aware of the fact that the calculation of the number of cycles until rupture goes beyond the range of the present theory. However, since the increase of the damage parameter beyond the state of critical damage D_{cr} is very rapid, especially for wider strain ranges (see Fig. 4), the results can be taken as a first approximation of the real situation. A typical evolution of the cyclic load test is presented in Fig. 5 as a plot of the stress versus strain. The test was carried out at $T = 627^{\circ}$ C and the specimen was strained in each cycle in the range $\varepsilon = \pm 3\%$. In Fig. 6 the final stress in each cycle at $\varepsilon = 3\%$ (i.e. before unloading was started) is plotted versus the number of cycles. Results for the elasto-viscoplastic damage analysis are compared to results obtained in the pure elasto-viscoplastic analysis. The decrease of the stress in the elasto-viscoplastic analysis can be explained by isotropic softening of the material (see also the hardening parameter R_1 in Table 1). Different results are obtained in the elasto-viscoplastic damage analysis. Here, the softening of the material is coupled to the effect of damage resulting in a rapid decrease of the final stress.

4. Conclusions

The present numerical model of material damage shows a fairly good agreement with the experimental results for cyclic loading until rupture, available in literature. However, the fundamental question, how general the model is with respect to different kinds of metals of the considered class, remains open. Also, for the time being, the restricted number of exclusively uniaxial numerical tests seems to be insufficient to draw general conclusions as to the exactness of the model for more general loading situations. Nevertheless, the obtained results encourage the authors to continue the outlined research on a broader experimental data basis with the perspective of an implementation of the proposed model in a more general FEM code.

References

1. G. Amar and J. Dufailly, *Identification and validation of viscoplastic damage constitutive equations*, Eur. J. Mech., A/Solids, **2**, 12, 197–218, 1993.

2. J. Lemaitre and J.-L. Chaboche, *Mechanics of solid materials*, Cambridge University Press, Cambridge 1990.

3. J.-L. CHABOCHE, *Continuous damage mechanics – a tool to describe phenomena before crack initiation*, Nucl. Engng. Des., **64**, 233–247, 1981.

4. J.-L. CHABOCHE, *Anisotropic creep damage in the framework of continuum damage mechanics*, Nucl. Engng. Des., **79**, 309–319, 1984.

5. J.-L. CHABOCHE, *Continuum damage mechanics: present states and future trends*, Nucl. Engng. Des., **105**, 19–33, 1987.

6. J. LEMAITRE, *A continuous damage mechanics model for ductile fracture*, J. Engng. Mater. & Tech., **107**, 83–89, 1985.

7. S.R. BODNER and K.S. CHAN, *Modeling of continuum damage for application in elasto-viscoplastic constitutive equations*, Engng. Fracture Mech., **25**, 5/6, 705–712, 1986.

8. M. KLEIBER and F.G. KOLLMANN, *A theory of viscoplastic shells including damage*, Arch. Mech., **45**, 4, 423–437, 1993.

9. A.L. GURSON, *Continuum theory of ductile rupture by void nucleation and growth*, Part I. *Yield criteria and flow rules for porous ductile materials*, Trans. ASME, J. Engng. Mat. Technol., **99**, 2, 2–15, 1977.

10. Y.Y. ZHU and S. CESCOTTO, *A fully coupled elasto-viscoplastic damage theory for anisotropic materials*, Int. J. Solids Structures, **32**, 11, 1607–1641, 1995.

11. A.F. SALEEB and T.E. WILT, *Analysis of the anisotropic viscoplastic-damage response of composite laminates – Continuum basis and computational algorithms*, Int. J. Numer. Methods Engng., **36**, 1629–1660, 1993.

12. D. HOLLAND, X. KONG, N. SCHLÜTER and W. DAHL, *Investigations concerning quantitative determination of local damage in ductile materials*, Steel Research, **8**, 361–367, 1992.

13. B. WESTERHOFF, *Eine Untersuchung zum geschwindigkeitsabhängigen Verhalten von Stahl*, Mitteilungen aus dem Inst. für Mech. Ruhr-Universität Bochum, **99**, 1995.

14. A. BJÖRCK and G. DAHLQUIST, *Numerical methods*, Prentice-Hall 1974.

15. P. KŁOSOWSKI, K. WOŹNICA and D. WEICHERT, *Vibrations of the elasto-viscoplastic truss element* [submitted to Computer and Structures].

16. P. KŁOSOWSKI, K. WOŹNICA and D. WEICHERT, *Dynamics of elasto-viscoplastic plates and shells*, Arch. Appl. Mech., **66**, 326–345, 1995.

GDAŃSK UNIVERSITY OF TECHNOLOGY, GDAŃSK

e-mail: klosow@pg.gda.pl

and

RWTH – AACHEN, UNIVERSITY OF TECHNOLOGY, AACHEN, GERMANY

e-mail: weichert@iam.rwth-aachen.de

Received November 4, 1996.